International Journal of Geophysics and Geochemistry
2017; 4(1): 1-17
http://www.aascit.org/journal/ijgg
ISSN: 2381-1099 (Print); ISSN: 2381-1102 (Online)

American Association for Science and Technology

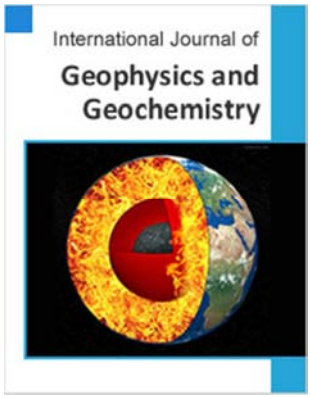

Keywords
Seismic Refraction,
Structural Modeling,
Tomography,
Faults,
Traveltime, Geoseismic Velocity

Received: March 21, 2017
Accepted: March 31, 2017
Published: June 7, 2017

Structural Modeling of Seismic Refraction Investigations at Wadi Beda El Atshan Area in the Eastern Desert, Egypt

Samir Riad[1], Assem E. El-Haddad[1], Mahmoud A. Abbas[2], Amany H. Said[1, *]

[1]Geology Department, Faculty of Science, Assiut University, Assiut, Egypt
[2]Geology Department, Faculty of Science, South Valley University, Qena, Egypt

Email address

amany_geophysics@yahoo.com (A. H. Said)
[*]Corresponding author

Citation

Samir Riad, Assem E. El-Haddad, Mahmoud A. Abbas, Amany H. Said. Structural Modeling of Seismic Refraction Investigations at Wadi Beda El Atshan Area in the Eastern Desert, Egypt. *International Journal of Geophysics and Geochemistry*. Vol. 4, No. 1, 2017, pp. 1-17.

Abstract

Seismic refraction tomography is an effective tool for determination of 2D velocity models and interface structures of the subsurface geologic section. The seismic refraction tomography was employed at Wadi Beda El Atshan area, near Quseir city in the Eastern Desert, Egypt. The study was conducted to: 1) construct the 2D structural model, 2) infer the downward extension of the observed surface faults, 3) obtain more information about the subsurface fault morphology and 4) detect the depth to the basement complex and delineation of its relief. The refraction data were collected in P-wave mode twice (direct and reverse) using the 24 channel seismograph (geode) along five profiles covering the study area. The obtained data were processed using two available software (GODOGRAF and SeisImager 2D). Seismic velocity field models, structural sections and, consequently geoseismic velocity sections were constructed. The interpreted 2D seismic models reveal up to three seismic zones with velocity ranging from less than 1000 to more than 4000 m/s. These zones display significant structural complexities where large fault blocks were interpreted. The models are clearly imaged several subsurface fault planes where some of them consider an extension of observed surface faults. The depth to the basement ranges from 0 to 190 m increasing toward the northwest direction. So, the applied 2D inversion of refraction traveltime curves has proved very effective in confirming the significance of suspected faults, facilitating the accurate setting and providing valuable deeper information about fault morphology.

1. Introduction

Seismic methods provide data that can provide important information about the subsurface condition including structure and distribution of rock types [1]. The medium where the seismic waves are propagating can be represented by many forms that are generally called models. A model is a calculated representation of a medium that gives a simplified image of the real conditions [2]. Modeling can be used to test the validity of assumptions regarding the effect of changes in the geologic section.

Modeling or calculation of theoretical models that match the observed data is called inversion and include two procedures; forward and reverse modeling. The forward or iterative modeling is based on comparing the observed data in the field with calculated

data of a theoretical model computed based on geological concepts. Trial-and-error adjustments of the medium parameters are made until the theoretical data agrees with the measured data. Inverse modeling provides a mathematical framework to construct models of some physical quantity based on measured data i.e. a model is derived directly from the observed data by mathematical means.

The aim of the present study is to construct 2D structural models of seismic refraction data in Wadi Beda El Atshan, Eastern Desert, Egypt to obtain more information about the subsurface fault morphology, to infer the downward extension of the observed surface faults, to detect the depth to the basement complex and delineation of its relief. The previous interpretations [3-8] concluded that the study area affected by transverse fractures oriented perpendicular to the Red Sea and affected by a set of faults which oriented in NW- SE, NE-SW, NNE-SSW, ENE-SWS, WNW-ENE, N-S and E-W directions. Here a detailed seismic refraction survey to study the existing structures at the study area. The collected data were interpreted using two different 2D refraction tomographic algorithms.

2. Geologic Setting

Wadi Beda El Atshan area is located to the south of Quseir– Qift road, about 10km west of Quseir city between latitudes 26^0 00 ′ and 26^0 06′ N and longitudes 34^0 08 ′ and 34^0 15′ E (Figure 1). The study area was chosen for its excellent exposure of tilted basement blocks and their Cretaceous to Tertiary sedimentary covers and including complex different structures represents proper example for the study objectives.

The geological studies in the studied area began in the early 20^{th} century, when the science of geology was at its infancy in Egypt. The inception of this phase of geological research [9] which was followed by many enthusiastic works. Most of special attention was also paid to the phosphate deposits in the area. These studies represent the majority of the previous works carried out on the studied area. Several authors studied this area as followed [10-29]. Generally, the deposits of Wadi Beda El Atshan (Figure 2) and the surrounding areas consist of, from base:- Precambrian crystalline basement (metavolcanics, metasediments and granitoid intrusives; [30, 31]), following a long period of quiescence, Upper Cretaceous to Eocene called pre-rift sediments (Nubia, Quseir, Duwi, Dakhla, Tarawan, Esna and Thebes formations; [24, 25) were deposited unconformably over the Precambrian basement. The pre-rift sediments appear as isolated sedimentary bodies forming two belts trending in a sub longitudinal direction parallel to the red sea coast.

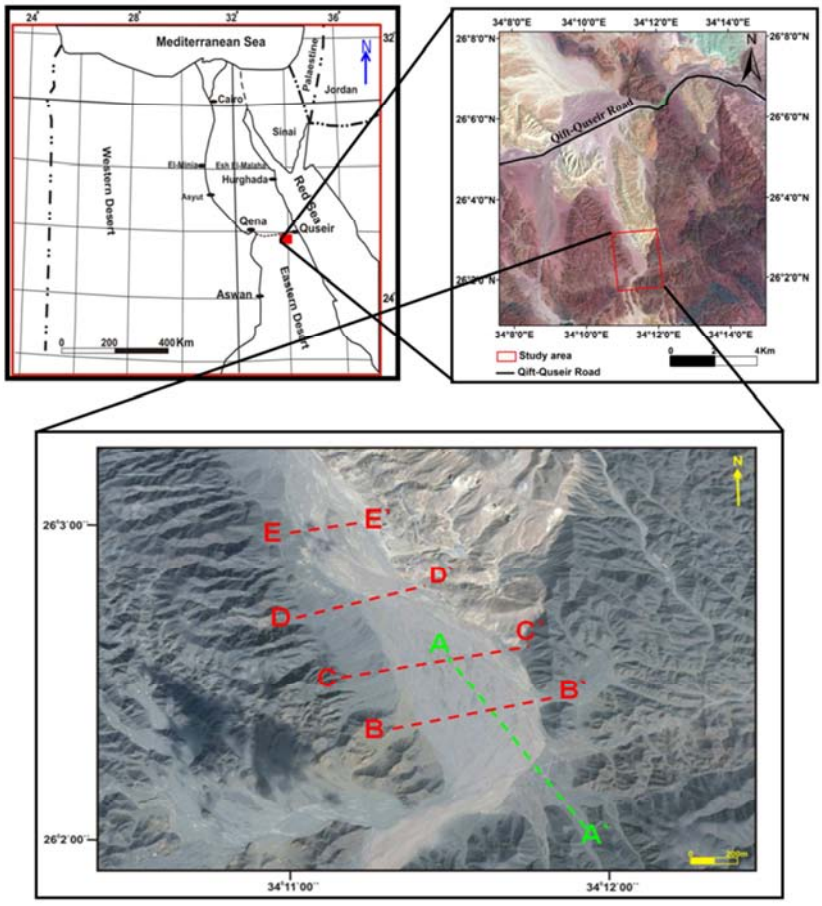

Figure 1. *Location map of the study area showing the seismic profiles.*

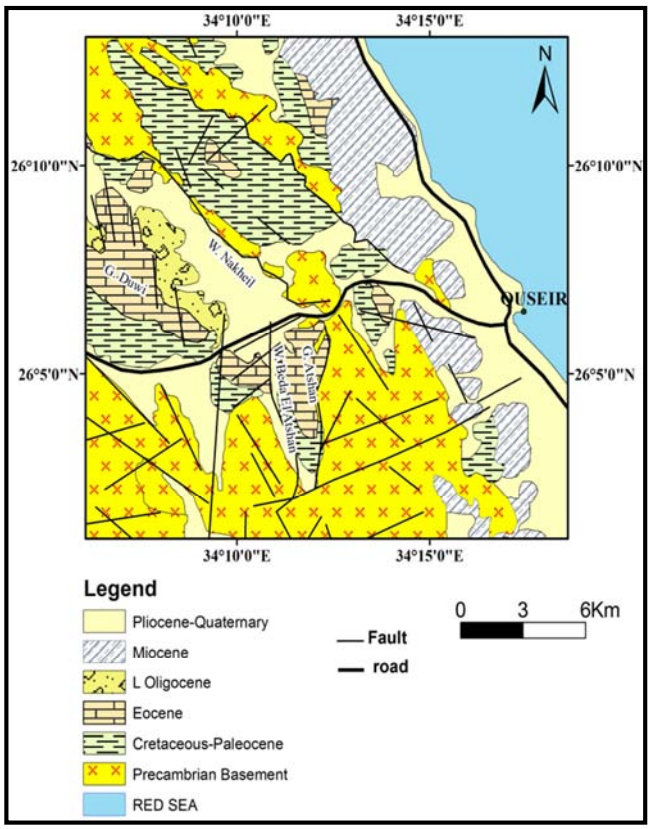

Figure 2. *Geological map at the study area (After Khalil and McClay, 2002 [6]).*

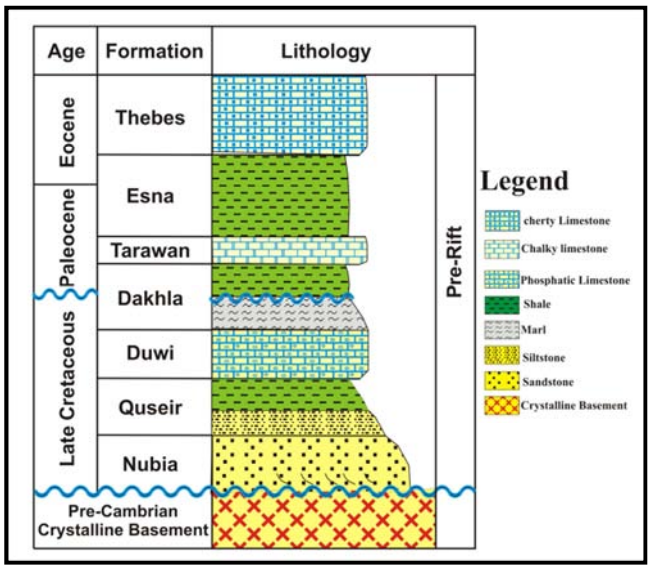

Figure 3. *Stratigraphic sequence at the study area (After Said, 1990 [31]).*

3. Methodology

Two available software (GODOGRAF and SeisImager 2D) were used for interpretation of the seismic refraction data and construct the structural models. These programs depend mainly on curved ray paths of the seismic waves.

The first algorithm (GODOGRAF) is based on a local approximation of the real velocity distribution by homogeneous functions of two coordinates [32, 33]. In this inversion the preliminary distinguishing and identification of waves on travel time curves from different interfaces are automatically performed. Whereas, for two reverse travel time curves the non-linear transformations continuously convert the direct travel time curve to the reverse one and vice versa [32, 33]. The output of this algorithm was presented as a velocity field section, and a structural section.

The other algorithm (SeisImager 2D) is based on the tomographic inversion technique which involves the creation of an initial velocity model, then iteratively tracing rays through the model, comparing the calculated traveltimes to the measured traveltimes, modifying the model, and repeating the process until the difference between calculated and measured times is minimized.

4. Field Work

Shallow seismic refraction measurements have been acquired along five profiles in the study area Fig (1). The measured profiles were oblique and/or perpendicular to the axes of selected observed surface faults oriented in different directions at the study area, were distributed to cover the study area to give a complete image for existing structures in the region. The length of these profiles was varied based on the geologic conditions of the area.

a) The first profile (AA') is oriented NW-SE parallel to the main direction of the Wadi Beda El Atshan at the end of the valley, consisted of two spreads (830m, 590m length), and the total length was 1070 m with 108 geophones, While the others (B-B', C-C', D-D' and E-E`) were oriented WSW-ENE perpendicular to the main stream of the valley with varied lengths.
b) The second profile (B-B') consisted of a one spread 800 m long with 91geophones were arranged in-line along this spread.
c) The third profile (C-C`) measured parallel to the third one at 255 m to the north of it. It consisted of one spread with total length of about (950m) and 96 geophones.
d) The fourth Profile (D-D') measured at the same direction at 510m to the north of the (C-C`) profile. It has total length of about 710 m and 71 geophones.
e) The last profile (E-E`) measured at the same direction at 530 m to the north of the (D-D') profile. Its total length is 470m and 48 geophones.

Refraction data were collected in P-wave mode twice (direct and reverse shot points), which the shot point-geophone arrangement is in the form of end-one offset spreads with adequate energy sources at one end of the line, and then at the other end. This is useful in determining the subsurface layer conditions and true velocities. The arrival times were conducted by 24 channel seismic geode manufactured by Geometrics with length of a geophone cable (240m). Heavy weight dropper with changing weights was used as energy source [34, 35]. Seismic events were picked

from 14 Hz vertical geophones oriented vertically to the seismic line at 10 m interval.

For each profile all obtained seismograms can be fixed together, taking into account the delay time, in order to obtain a complete continuous seismogram of n-channel as illustrated in the examples of direct and reverse seismic records shown in Figure (4). Acquisition parameters on the seismograph included filter setting, 0.5 seconds as record length and a 0.125 second sample rate. The obtained signal-to-noise ratio of the first arrivals was fairly good.

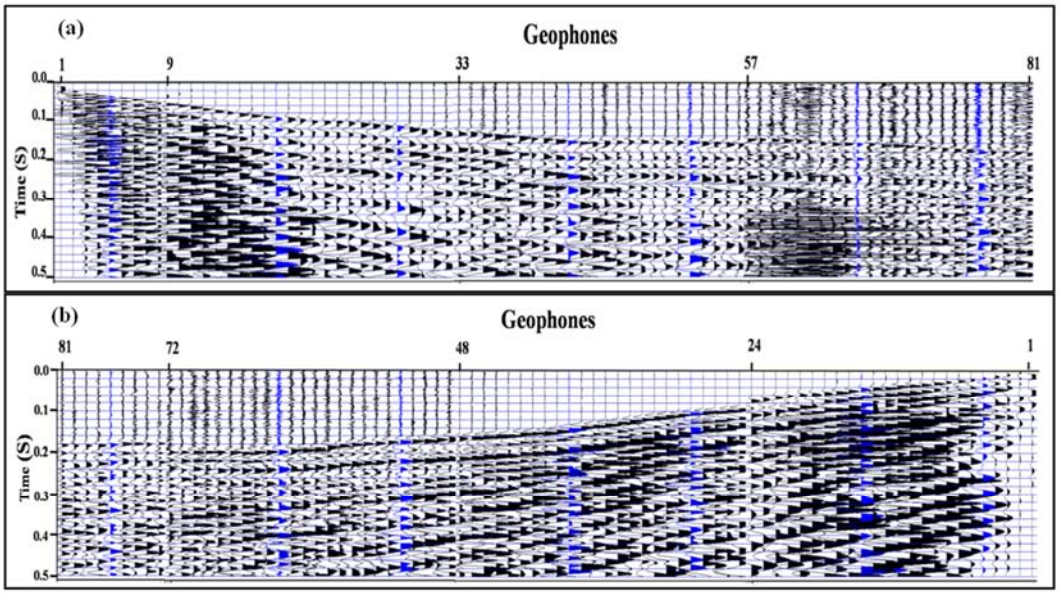

Figure 4. *A composite seismic record along the profile (B-B`); a) Forward shooting b) Reverse shooting.*

5. Results and Discussions

The registered digitized first arrival times of the seismic signals (P-waves) were plotted versus the distances along the seismic profiles figures (5, 8, 11, 14, 17). From these relations, it is clearly that; the reversed travel time curves are asymmetric and, the point of their intersection is shifted at the middle distance between the shots towards the side of lower velocity. It is evident that the first arrivals of the P-waves are related to the type of refracted waves with the curved ray paths in 2-D inhomogeneous medium [36-38].

The plotted time-distance graphs of the collected data were interpreted using 2-D refraction tomographic inversion algorithm (GODOGRAF) and 2-D inversion tomographic technique (SeisImager 2D).

The resultant 2-D velocity field models of the five measured profiles form GOODGRAF program are presented in figures (6a, 9a, 12a, 15a, 18a) and from SeisImager 2D program are presented in figures (7a, 10a, 13a, 16a, 19a). These models are displayed as fields of velocity contour lines with a constant interval (500 m/s). Furthermore, structural sections, where the same velocity field is represented as a surface with the shaded relief overlapped by velocity contour isolines, are also presented in figures (6b, 9b, 12b, 15b, 18b). From these lines, a visual estimation of the velocity gradient values is possible because the gradient is inversely proportional to distance between contours. These structural sections allow a sight of boundaries and blocks limited by faults. So, at these images, the seismic boundaries and faults can be allocated. The greatest illumination (brighter lines) corresponds to transition zones where the velocity increases with depth and the lowest illumination (dark lines) corresponds to inversion discontinuities (tops of thin waveguides). The seismic zones, which may represent the layers or strata, can be identified by extended boundaries and maintaining the values of the velocity gradient and velocity interval from top to bottom of layer [32, 33]. Otherwise, constructed geoseismic velocity sections from GOODGRAF and SeisImager 2D are also prepared in (Figs. 6c, 9c, 12c, 15c, 18c) (Figs. 7b, 10b, 13b, 16b, 19b) respectively. The non-uniform depths of the sections are due to non-uniform penetration of seismic rays which are calculated during the solution of the inverse problem.

Using the above mentioned criteria, three seismic zones were allocated in the enclosing rocks covered by irregular thickness of the surface layer (Figs. 6c, 9c, 12c, 15c, 18c) (Figs. 7b, 10b, 13b, 16b, 19b). This surface layer is characterized by constant high gradient and velocity less than 1000m/s. Otherwise, each of the seismic zones has its own constant value of velocity gradient and constant velocity range.

The uppermost seismic zone is characterized by constant low gradient and velocity ranging from 1000 to 2000 m/sec. The second seismic zone has a relatively more gradient and velocity range 2000- 4000 m/s. The third seismic zone is characterized by high gradient and velocity more than 4000 m/s. These zones which may represent sedimentary layers and the bed rock are designated with different color shading in the structural geoseismic sections.

Moreover, a high degree of faulting is suggested from seismic data where significant lateral velocity variations exist

along these profiles [39-43]. Likewise, the discontinuous nature of first-breaks in the seismographs (Figure 4) and the gap in the time distance curves at the same distance (Figs. 5, 8, 11, 14, 17), indicate variability in the subsurface layers. This discontinuity is reflected in the interpreted seismic models, velocity field models and structural sections, as abrupt lateral change in the velocity value [34, 38].

The detailed description of the geoseismic models around the study area is as follows:

Geoseismic velocity model along the profile A-A'

Inspection of the profile illustrates:

a) Only three seismic zones were distinguished along this profile, covered by (0-20 m thick) horizontal surface layer (Figure 6c, 7b). The surface coincides with the velocity isoline 1000 m/s.
b) The uppermost seismic zone has a maximum thickness about 50 m near the north western end decreasing to the south eastern direction until reaching about 5 m. The first interface, (bottom of this zone) is coinciding with the velocity isoline 2000 m/s. It is found at depth 10m to the south eastern direction increasing toward north western direction reaching 90 m due to eight normal faults.
c) The second seismic zone has average thickness from 15 to 75 m.
d) The depth to the third seismic zone i.e. second interface (with a mark 4000 m/sec.) is found at about 25 m near the south eastern end and increasing north western ward to150 m.
e) There are eight normal faults influence on this profile, probably parallel, with their down throw from SE to NW as follow; 25m, 40m, 25m, 15m, 15m, 30, 30 and 25m.
f) The second fault from SE coincides with the traced of ENE-WSW surface fault. As well, the fourth fault from SE coincides with another traced ENE-WSW surface fault at a distance up to 450m from the SE end.

Geoseismic cross section along BB` profile:

From the velocity models, structural model, and geoseismic cross sections (Figure 9c, 10b) it is clear that three seismic zones are revealed along this profile covered by 0-10 m thick of the surface layer. Most of these zones are affected by four fault planes which may represent the downward extension of two observed surface fault and subsurface faults. Whereas, at point 235 m from the ENE end, which might be at the intersection with the NE surface fault (Gebel Atshan Fault Zone), steeply northwest dipping normal fault plane was detected. It has a vertical displacement about 35 m. Around the point 70m from the WSW end, there is a gentle north east dipping fault plane (listric fault) which intersect with the second NW surface fault, its vertical displacement about 35m.

Also there are two subsurface steeply northwest dipping normal fault plane was detected with vertical displacement 15 and 20m. Due to the presence of these faults, the section along BB` profile seems to be subdivided into four blocks where, the depth to basement is found at different levels as follows:

g) The basement surface is detected at depth 15m in the first ENE block, at 30m in the second block, at 90m in the third block and at 30 m in the fourth block in WSW end.

Geoseismic section along profile CC`:

Along this profile, the seismic zones are clearly distinguished covered by 0-10 m thick of the surface layer (Figure12c, 13b). Otherwise, five fault planes are noted along it. The first fault is detected directly beneath NE surface fault (Gebel Atshan Fault Zone) at point 15m from the ENE end at the surface contact between the basement complex and the overlaying sedimentary cover. It is steeply north-west dipping normal fault plane was detected. It has a vertical displacement about 35 m. Around the point 230m from the WSW end, there is a gentle north east dipping fault plane (listric fault) which intersect with the second NW surface fault, its vertical displacement about 35m. There is another subsurface steeply north-west dipping normal fault plane was detected with vertical displacement 25m. Also there are two subsurface a gentle north east dipping normal faults (listric faults) was detected with vertical displacement 20 and 30m. Due to the presence of these faults, the section along CC` profile seems to be subdivided into six blocks where, the depth to basement is found at different levels as follows:

h) The basement surface is detected at depth 80m in the first ENE block, at about 95m in the second block, at 145m in the third block, at 120 m in the fourth block, at 95 m in the fifth and at 30 m in the sixth block in WSW end.

Geoseismic cross section DD`:

Three seismic zones are delineated along this profile covered by 0-10 m thick of the surface layer (Figure15c, 16b). These zones are affected by gentle northeast dipping fault plane (listric fault) which intersects with the NW surface fault at the point 215m from the WSW end. Its vertical displacement is about 30m. Due to the presence of this fault, the section along DD` profile seems to be subdivided into two blocks where, the depth to basement is found at different levels as follows:

i) The basement surface is detected at depth 190 m in the first ENE block and at about 95m in the second block in WSW end.

Geoseismic cross section EE`:

Along this profile, the seismic zones are detected covered by about 18 m surface layer (Figure18c, 19b). These zones are affected by gentle northeast dipping fault plane (listric fault) which intersects with the NW surface fault at the point 135m from the WSW end. Its vertical displacement is about 15m. Due to the presence of this fault, the section along EE` profile seems to be subdivided into two blocks where, the depth to basement is found at different levels as follows:

j) The basement surface is detected at depth 160 m in the first ENE block and at about 85m in the second block in WSW end.

Profile (A-A`):

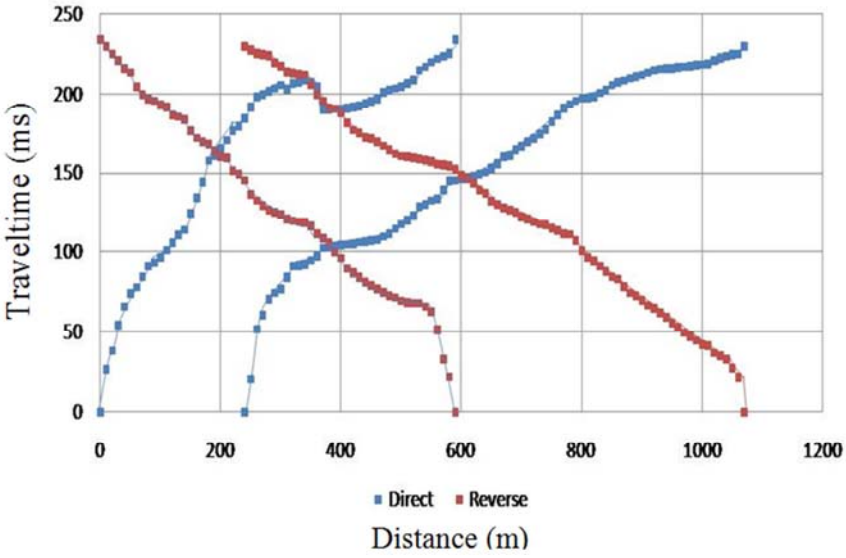

Figure 5. *Time-distance curve along profile (A-A`).*

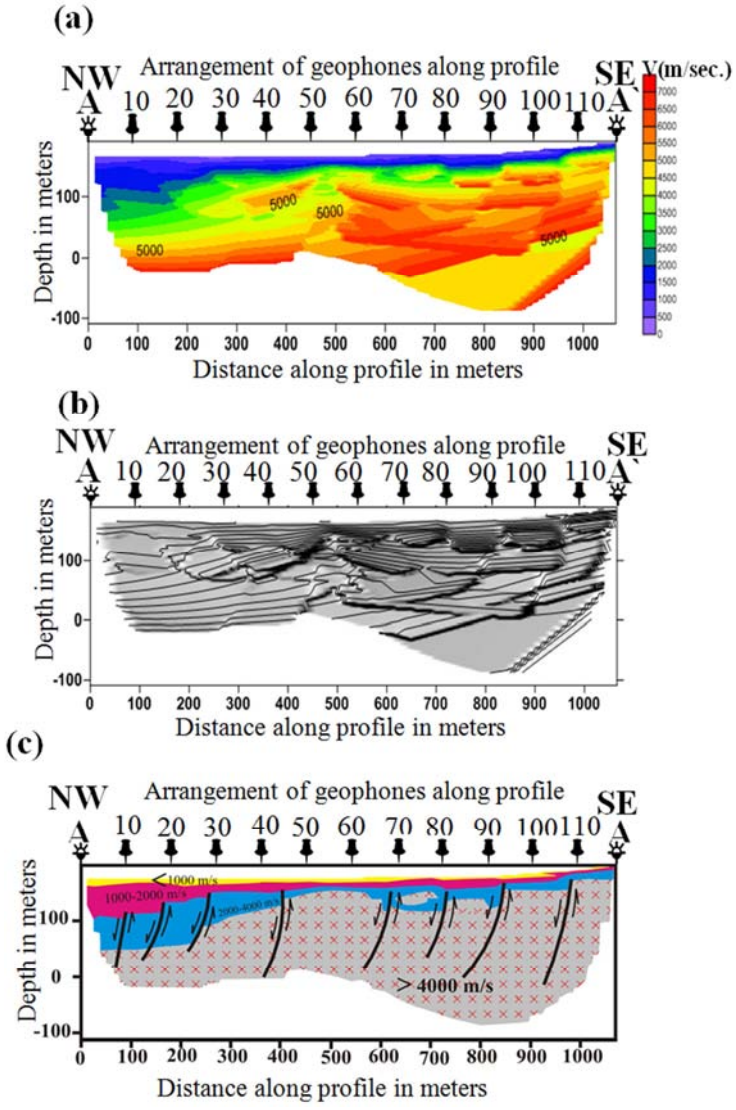

Figure 6. *Results from GODOGRAF program: a) 2D velocity section, b) 2D structural section, c) 2D geoseismic velocity section.*

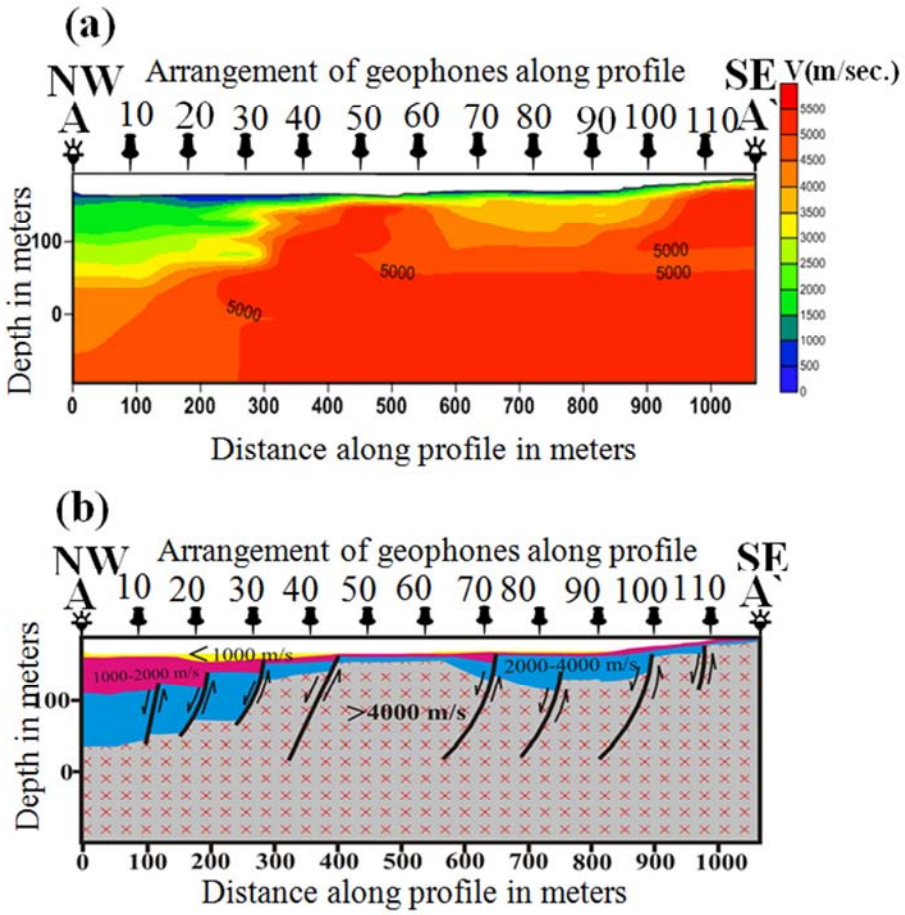

Figure 7. *Results from SeisImager 2D program: a) 2D velocity section, b) 2D geoseismic velocity section.*

Profile (B-B`).

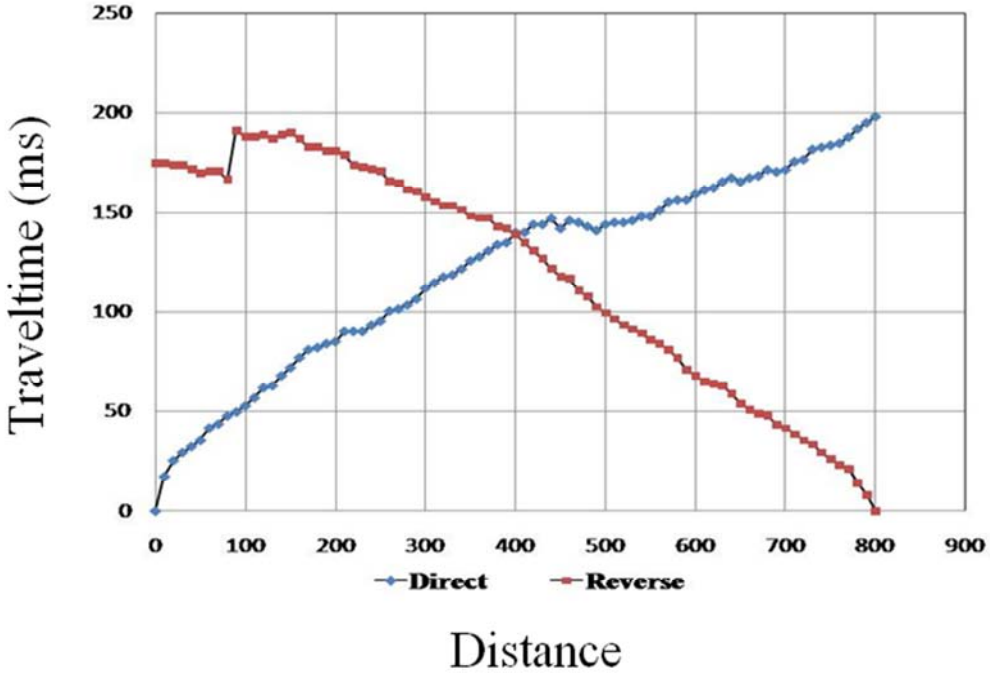

Figure 8. *Time-distance curve along profile (B-B`).*

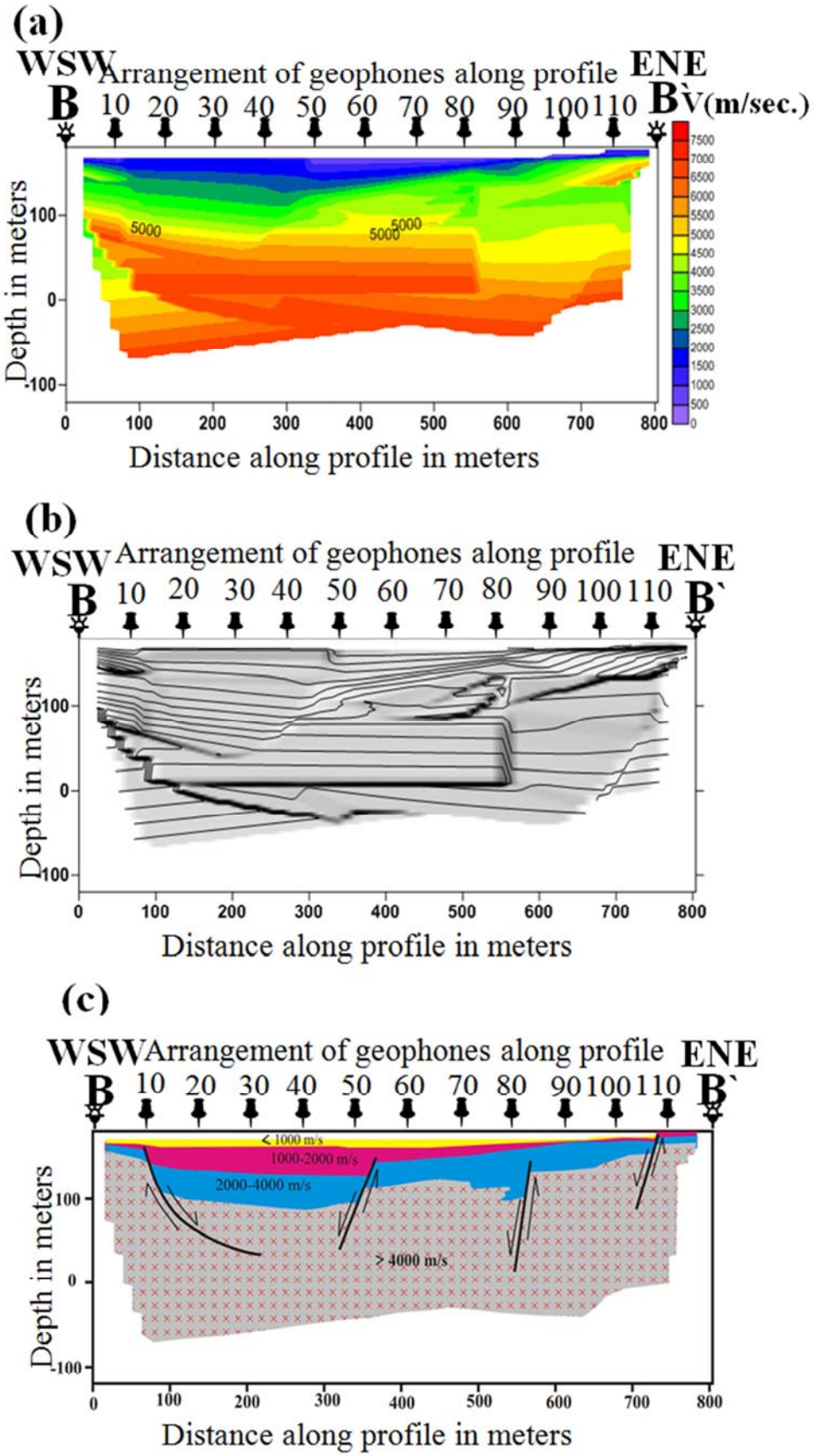

Figure 9. *Results from GODOGRAF program: a) 2D velocity section, b) 2D structural section, c) 2D geoseismic velocity section.*

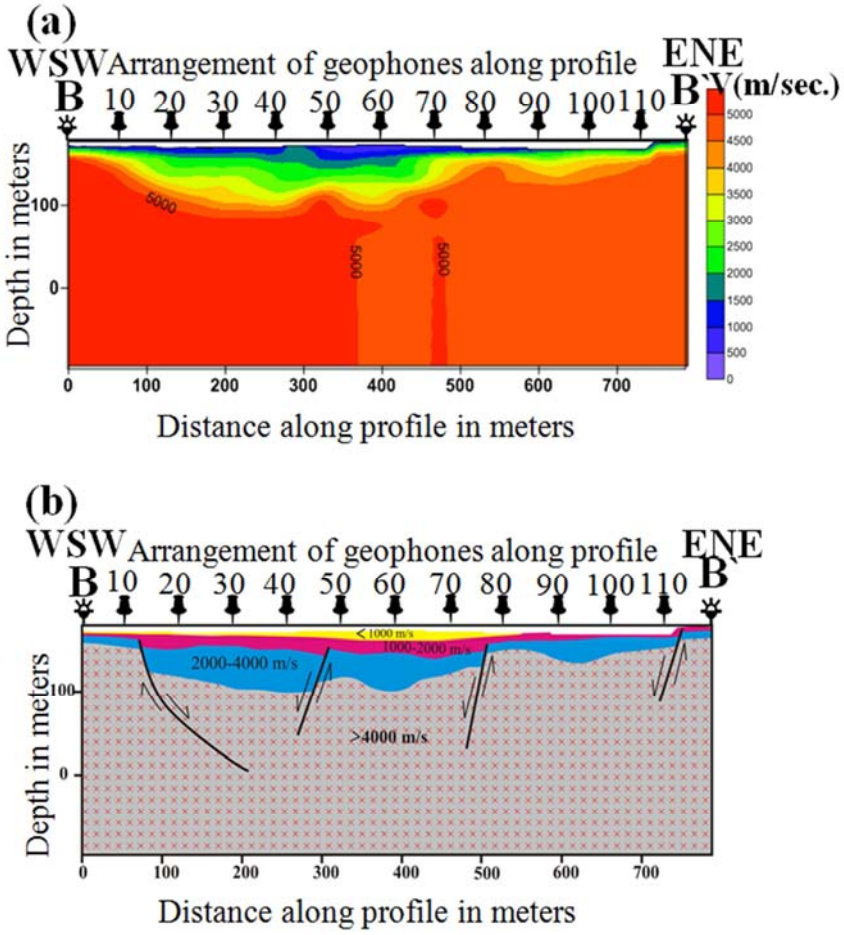

Figure 10. *Results from SeisImager 2D program:a) 2D velocity section, b) 2D geoseismic velocity section.*

Profile (C-C`):

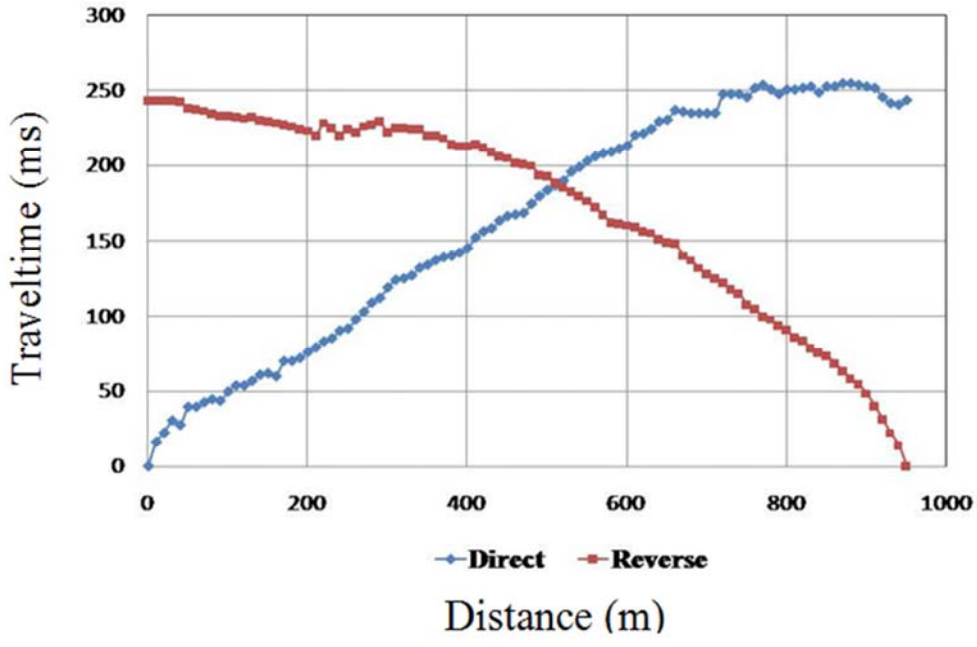

Figure 11. *Time-distance curve along profile (C-C`).*

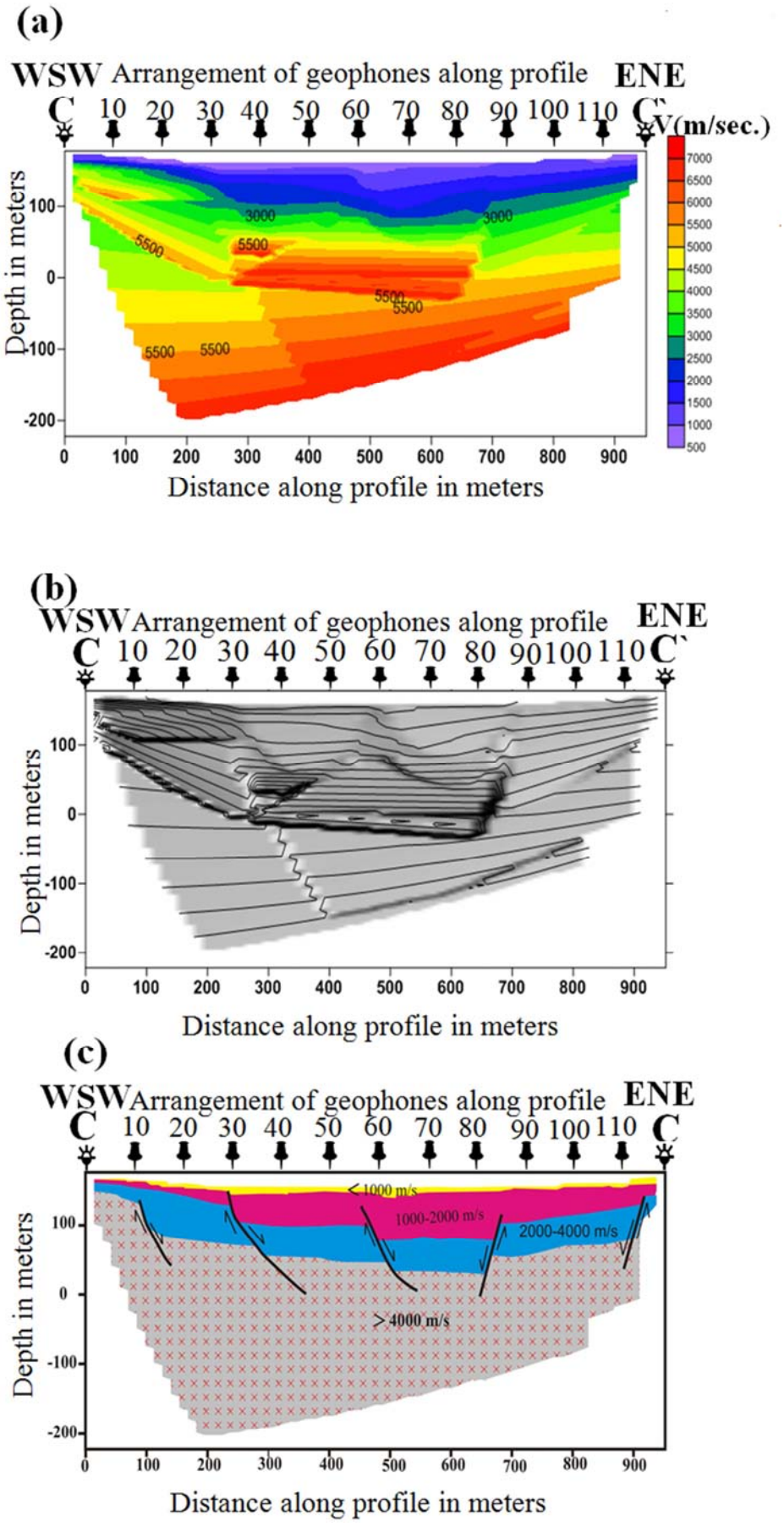

Figure 12. *Results from GODOGRAF program: a) 2D velocity section, b) 2D structural section, c) 2D geoseismic velocity section.*

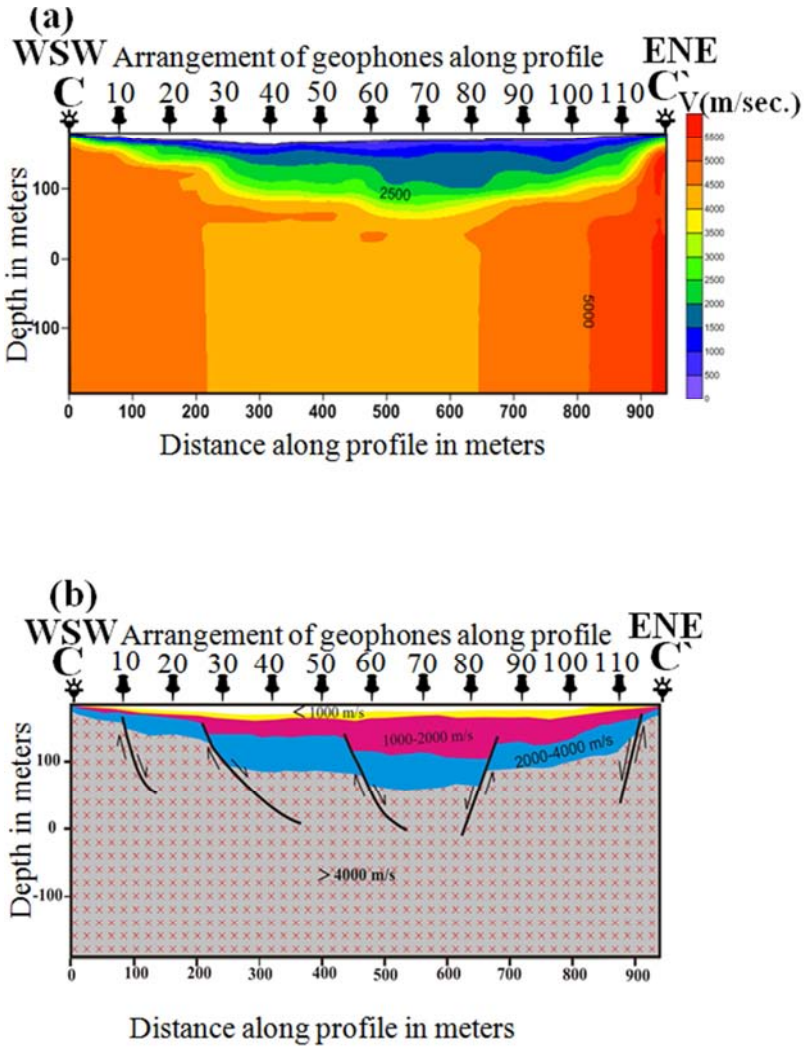

Figure 13 *Results from SeisImager 2D program: a) 2D velocity section, b) 2D geoseismic velocity section.*

Profile (D-D`)

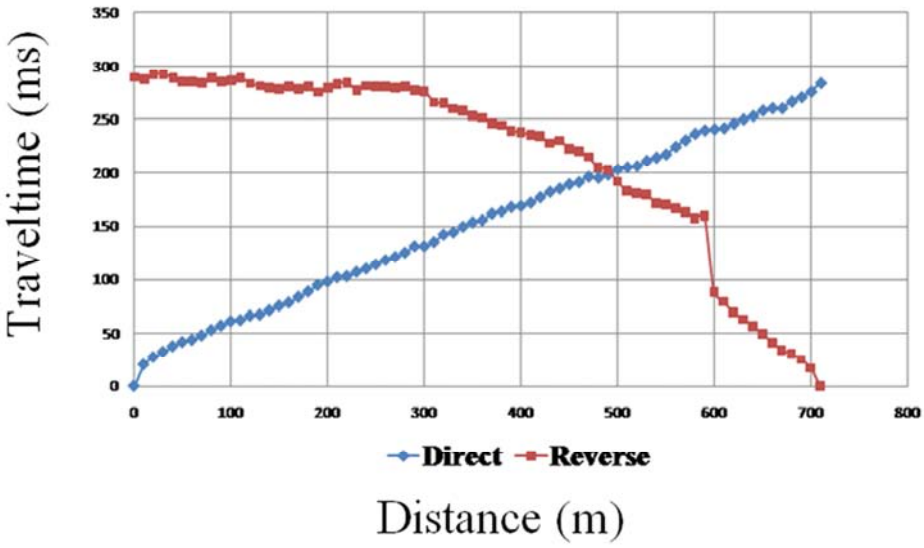

Figure 14. *Time-distance curve along profile (D-D`).*

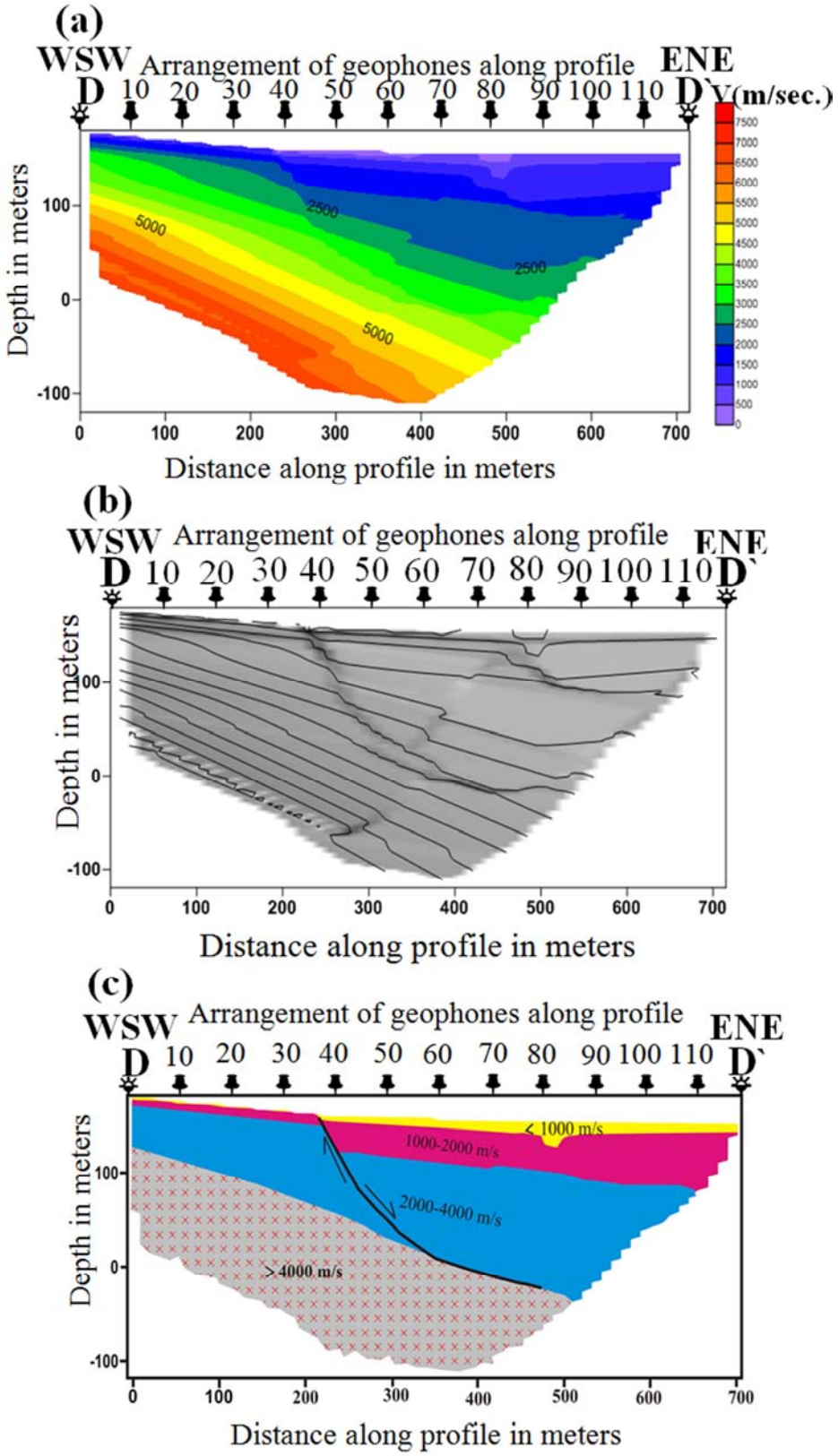

Figure 15. *Results from GODOGRAF program: a) 2D velocity section, b) 2D structural section, c) 2D geoseismic velocity section.*

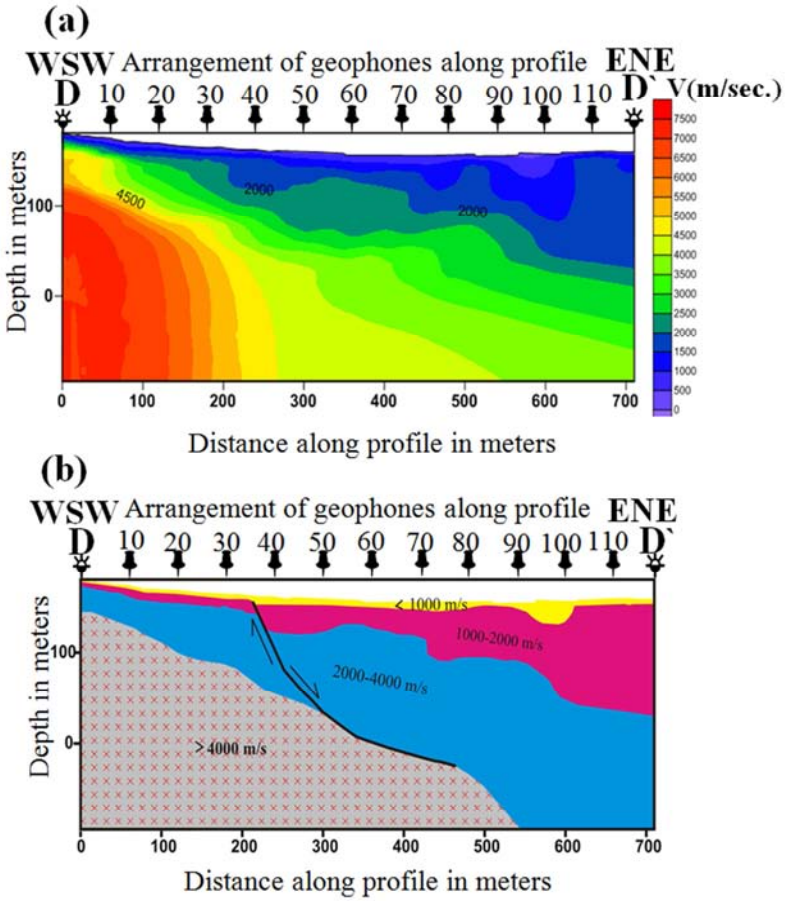

Figure 16. *Results from SeisImager 2D program: a) 2D velocity section, b) 2D geoseismic velocity section.*

Profile (E-E`):

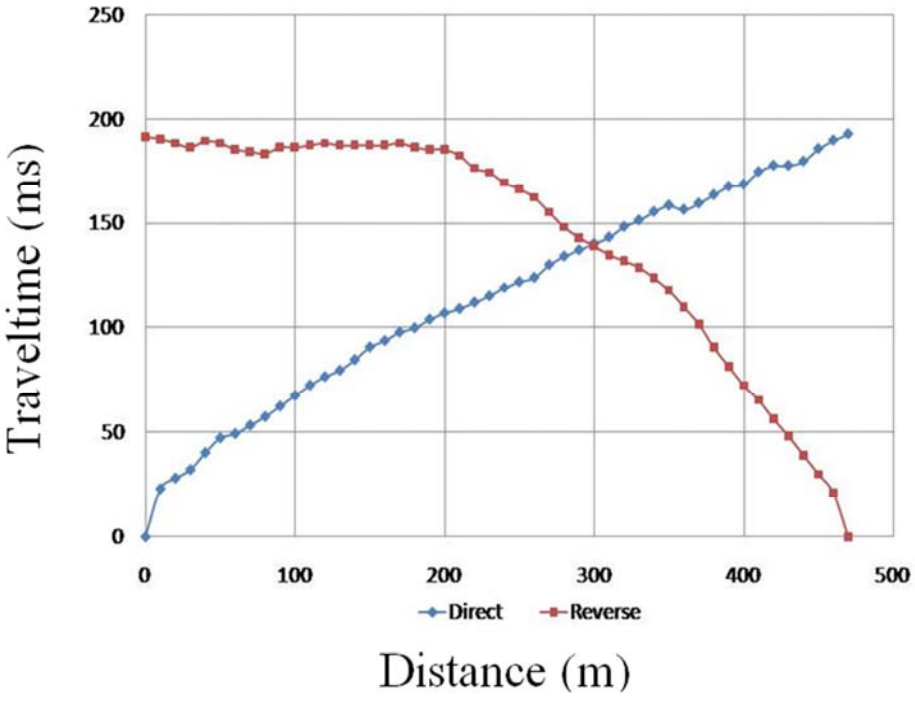

Figure 17. *Time-distance curve along profile (E-E`).*

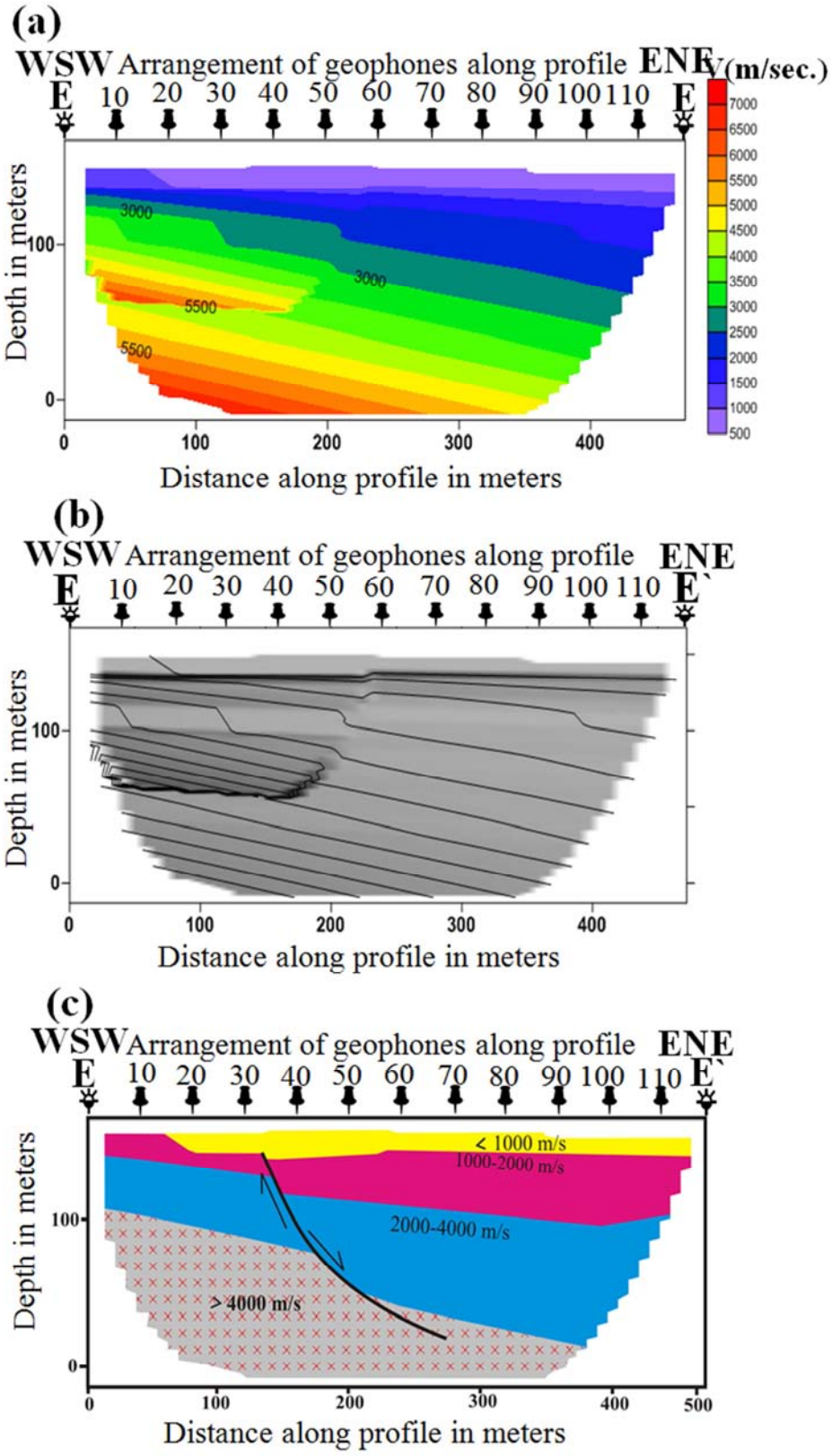

Figure 18. *Results from GODOGRAF program: a) 2D velocity section, b) 2D structural section, c) 2D geoseismic velocity section.*

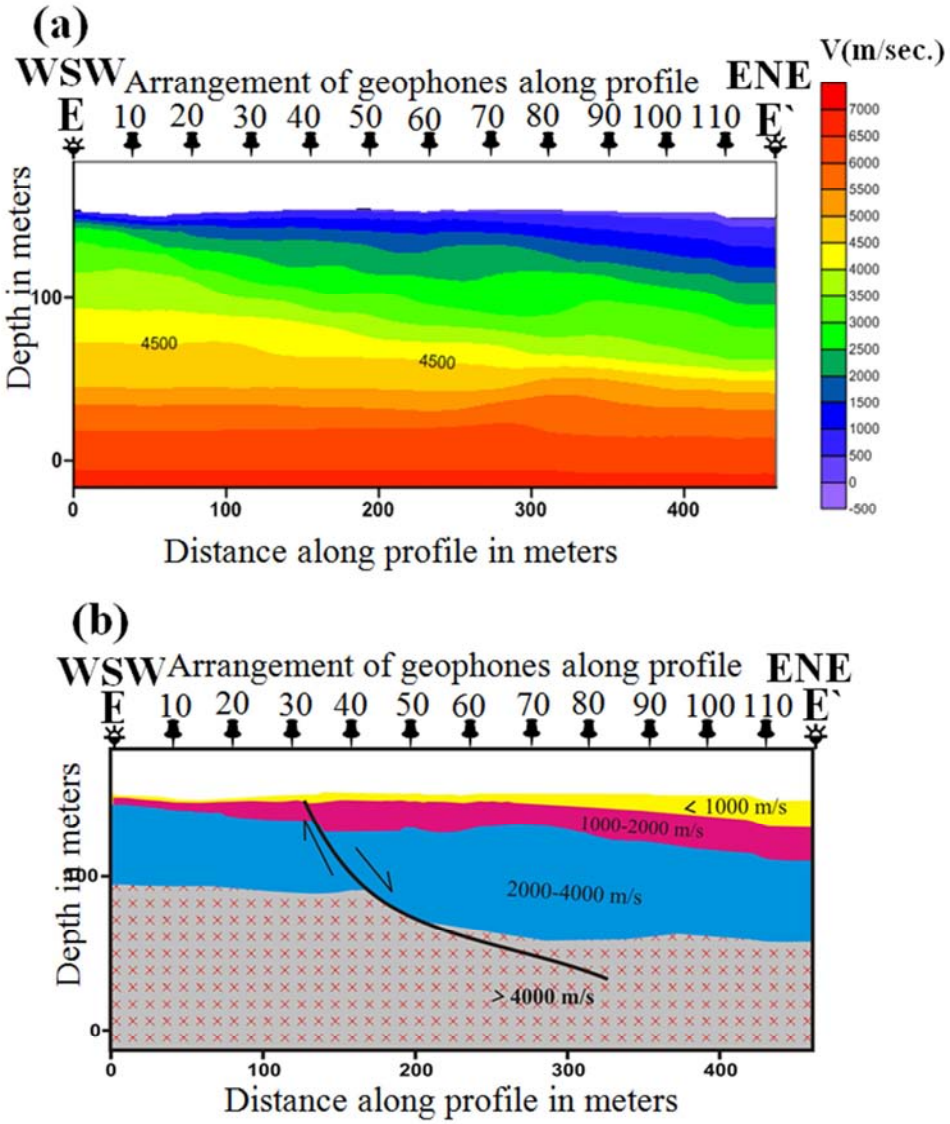

Figure 19. *Results from SeisImager 2D program: a) 2D velocity section, b) 2D geoseismic velocity section.*

6. Conclusions

Generally, the careful inspection of the resultant 2-D velocity models around the study area shows the following notable remarks;

a) The obtained results from both GODOGRAF and SeisImager 2D program are relatively similar.

b) The interpreted geoseismic models contain valuable deduced information on the: geological succession velocities, depth to basement complex and the prevailing structures.

1. The seismic models reveal multi-layer section of three geoseismic layers according to their velocity characteristics.
2. The velocity values ranging from less than 1000 to more than 4000 m/s within the time interval of about 300 msec. This range of velocity characterizes basement rocks and the overlying sedimentary sequence. The distribution of these velocities indicates that the studied subsurface sections seem to have strong anisotropic medium in both vertical and lateral directions.
3. The maximum penetration of the P-wave reached more than 250m in some profiles.
4. The depth to the basement (consequently the thickness of the sedimentary succession) varies from 5 to 190 m in northwest direction.
5. The study area displays significant structural complexities, where large fault blocks are interpreted delineating tilted fault blocks (half graben structure). A high degree of faulting is suggested from seismic data where significant lateral velocity variations exist along these profiles.
6. The area was affected by a set of faults oriented in NW-SE, NE-SW, ENE-WSW directions. The NW- SE fault direction is a listric fault (the dip angle decreases with depth) while NE-SW fault direction is steeply dipping normal fault so that this basin is considered a

symmetrical basin. On the other hand, the ENE-WSW fault direction coincides with ancient transverse fractures oriented perpendicular to the Red Sea.

7. The suspected surface fault planes are successfully detected and corroborated by the intersections locations of the detected fault planes with the surface. The different parameters of these faults are accurately determined. Moreover, there are some subsurface fault planes are also detected along AA`, BB` and CC` profiles.
8. The applied 2D inversion of refraction traveltime curves has proved very effective in confirming the significance of suspected faults and facilitating their accurate setting and morphology.

References

[1] Sheriff, R. E. and Geldart, L. P. (1995): Exploration Seismology (2nd. ed.). Cambridge. 628p.

[2] Sheriff, R. E. (2002): Encyclopedic Dictionary of Applied Geophysics. Society of Exploration Geophysicists. 235p.

[3] Garson, M. S. and Krs, M. (1976): Geophysical and geological evidence of the relationship of Red Sea transverse tectonics to ancient fractures, Geol. Am. Bull., V. 87, pp. 169-181.

[4] Valentine, M. J. (1985): Structure and tectonics of the southern Gebel Duwi area, Eastern Desert of Egypt, contribution no. 53, M.Sc Thesis, Department of Geology and Geography, University of Massachusetts, Amherst, 156pp.

[5] Moustafa, A. R. (1997): Controls on the development and evolution of transfer zones: the influence of basement structure and sedimentary thickness in the Suez rift and Red Sea. Journal of Structure Geology, V.19 (6), pp.755 -768.

[6] Khalil, S. M. and McClay, K. R. (2002): Extensional fault-related folding, northwestern Red Sea, Egypt. Journal of Structure Geology, V.24, pp. 743-762.

[7] Amer, R., Sultan, M., Ripperdan, R. and Encarnación, J. (2012): Structural Architecture for Development of Marginal Extensional Sub-Basins in the Red Sea Active Rift Zone. International Journal of Geosciences, V. 3, pp. 133-152.

[8] Metawi, M. M. A. (2017): Geophysical data interpretation of Duwi area, Central Eastern desert of Egypt. M.Sc. Thesis. Fac. of Sci. South Valley Univ., 118 pp.

[9] Barron, T. and Hume, W. F. (1902): Topography and Geology of Eastern Desert Of Egypt (Central Portion). Egypt. Surv. Dep. Cairo, 331p.

[10] Beadnell, H. J. L. (1924): Report on the Geology of the Red Sea coast between Quseir and Wadi Ranga. Petrol. Res. Bull., 13, Governmental Press, Cairo, 37p.

[11] Cox, L. R. (1929): Notes on the post-miocene Ostreidae and Pectinidea of the Red Sea region with remarks on the geological significance of their distribution. Proc. Malacol. Soc. London, V. 18, pp. 165-209.

[12] Cuvillier, J. (1930): Révision du nummulitique Egyptien. Mém. Inst. Egypte, Paper. 16, 371p.

[13] Nakkedy, S. E. (1949): The foraminiferal fauna of the Esna Shales of Egypt, Part I, Inst. Egypt, Bull., Cairo, V. 31, pp. 209-247.

[14] Nakkedy, S. E. (1950): A new foraminferal fauna from the Esna shales and Upper Cretaceous Chalk of Egypt. J. Paleon., V. 24, pp. 675-692.

[15] Nakkedy, S. E. (1952): The foraminiferal fauna of the Esna Shales of Egypt, Part 2, Inst. Egypt, Bull., Cairo, V. 33, pp. 397-430.

[16] Nakkedy, S. E. (1957): Biostratigraphy and inter-regional correlation of the Upper Senonian and Lower Paleocene of Egypt, J. Paleon., V. 31, pp. 428-447.

[17] Youssef, M. I. (1949): Stratigraphical Studies in Kossier area. Ph.D. Thesis, Alex. Univ., 285pp.

[18] Youssef, M. I. (1957): Upper Cretaceous rocks in Quseir area. Bull. Inst. Desert Egypt, V. 7, pp. 35-54.

[19] Abdou, H. F. (1955): Lateral Variations of some Upper Cretaceous rocks (Kosseir area), M.Sc. Thesis, Fac. Sci., Alex. Univ., 188p.

[20] Ghorab, M. A. (1956): A Summary of a proposed rock Stratigraphic classification for the Upper Cretaceous rocks in Egypt. April 9th. Geol. Soc. Egypt (Abstract).

[21] Abd El-Razik, T. M. (1967): Geological Studies of Sedimentary rock formations in Gebel Anz near Quseir (Eastern Desert, UAR). M.Sc. thesis, Fac. Sci., Cairo Univ, 184 p.

[22] Abd El-Razik, T. M. (1968): Stratigraphy of the Sedimentary cover of Anz-Atshan-south Duwi district. Bull. Fac. Sci. Cairo Univ., V. 41, pp. 153-179.

[23] Abd El-Razik, T. M. (1969): Stratigraphical Studies on the Phosphate deposits between River Nile and Red Sea (south latitude 27°N). Bull. Fac. Sci. Cairo Univ., V. 42, pp. 299-324.

[24] Issawi, B., Francis, M., El-Hinnawy, M., Mehanna, A. and El-Dafter, T. (1971): Geology of Safaga-Quseir coastal plain and of Mohamed Rabah area, Ann. Geol. Surv. Egypt, V. 1, pp. 1-9.

[25] Issawi, B. (1972): Review of the Upper Cretaceous-Lower Tertiary Stratigraphy in central and Southern Egypt, AAPG Bull., V. 56, pp. 1448-1463.

[26] Malak, E. M. (1980): Geological Studies on the Quseir area. Ph.D Thesis, Fac. Sci., Assuit Univ., 265pp.

[27] Mahran, T. M. (1997): Cyclicity in Nakheil Formation (Oligocene), West of Quseir, Red Sea, Egypt. Egyptian Journal of Geology. V. 41 (2A), pp. 309-346.

[28] Tantawy, A. A. (2003): Calcareous nannofossil biostratigraphy and paleoecology of the Cretaceous Tertiary transition in the central eastern desert of Egypt. Marine Micropaleontology. V. 47, pp. 323-356.

[29] Khalil, H., Fathy, M. S., Abdeldayem, A. L. and Ghobara O. A. (2016): Stratigraphical studies on the Upper Cretaceous - Lower Eocene rocks in Central Eastern Desert, Egypt. Delta Journal Science, V. 37, pp. 147-173.

[30] Akaad, M. K. and Noweir, A. M. (1980): Geology and lithostratigraphy of the Arabian desert orogenic belt between latitudes 25^0 35′ and 26^0 30′. Bull. Inst. Applied Geol., King Abdul Aziz Univ., Jeddah, V. 3 (4), pp. 127-135.

[31] Said, R. (1990): The Geology Of Egypt, Balkema, Rotterdam 734p.

[32] Piip, V. B. (2001): 2D inversion of refraction traveltime curves using homogeneous functions. Geophysical Prospecting, V. 49, pp.461-482.

[33] Piip V. B. and El-Haddad A. E. (2008): Automatic interpretation of shallow seismic data with homogeneous function method to investigate landslide body of Dallackau area, northern Ossetiya-Allaniya, Russia. J. Appl. Geophys., V.7, No.1, pp.321-337.

[34] El-Haddad, A. E. (2003): Development of a portable weight-dropper apparatus and field application in the Dakhla Oasis area, Western Desert, Egypt, Bull. Fac. Sci., Assiut Univ., 32(1-F), pp. 103-119.

[35] El-Haddad, A. E. M, Bakheit, A. A, Ibrahim, H. A., and Mewafy, F. M. (2006): Application of shallow seismic refraction method for investigation of the subsurface geologic section in the area between Tushka and Abu Simble, Western Desert, Egypt. Assiut Univ. J. of Geology, 35(2), pp. 125-140.

[36] Oblogina, T. I., and Piip V. B. (1974): Criteria for identification and interpretation method of seismic waves in the case of folded- block models of the earth's crust in collected methods of geophysical investigation of the oceans, Nauka, pp, 54-65 (in Russian) G. V.

[37] El-Haddad A. E. (2002): Application of seismic traveltime tomography to study the subsurface geologic sections in Kharga area, Western Desert, Egypt: "A Case Study". Bull. Fac. Sci., Assiut Univ, V. 31(1-F), pp. 153-165.

[38] Mewafy, F. M. (2007): Geophysical studies on Tushka-Abu simbel area, south western desert, Egypt. M.Sc Thesis, Dept. of Geology, Faculty of Science, Assiut Univ., 117p.

[39] Behera, L.; Sain, K.; Reddy, P. R., Rao, I. B. P. and Sarma, V. Y. N (2002): Delineation of shallow structure and the Gondwana graben in the Mahanadi delta, India, using forward modeling of first arrival seismic data. Journal of Geodynamics, V. 34, pp 127-139.

[40] Demanet, D.; Pirard, E.; Renardy, F. and Jongmans, D. (2001): Application and processing of geophysical images for mapping faults. Computers & geosciences, V. 27, pp 1031-1037.

[41] Holker, B. A., Holliger, K., Manatschal, G. and Anselmetti,F. (2002): Seismic reflectivity of detahment faults of the Iberian and Tethyan distal continental margins based on geological and petrophysical data. Tectonophysics., V. 350, pp. 127-156.

[42] Greenhalgh, S. and Zhou. B. (2002): Seismic refraction mapping of fracture swarm in the Western Coalfied of New South Wales, Australia. International Journal of Rock Mechanics and Mining Sciences, V.39, pp. 389-394.

[43] Mackenzie, G. D., Shannon, P. M., Jacof, A. W. B., Morewood, N. C., Makris, J. Gaye, M., Edandolff, F. (2002): The velocity structure of the sediments in the southern Rocall Basin: results from new wide angle seismic modeling., Marine and Petroleum Geology, V. 19, pp. 989-1003.